

*Journal of*  
***Mechanics of***  
***Materials and Structures***

**SHAPE OPTIMIZATION IN AN ELASTIC PLATE UNDER REMOTE  
SHEAR: FROM SINGLE TO INTERACTING HOLES**

Shmuel Vigdergauz

***Volume 3, N° 7***

***September 2008***



mathematical sciences publishers

## SHAPE OPTIMIZATION IN AN ELASTIC PLATE UNDER REMOTE SHEAR: FROM SINGLE TO INTERACTING HOLES

SHMUEL VIGDERGAUZ

An elastic plate with two closely spaced identical holes of fixed area is taken as a two-dimensional sample geometry to find the interface shape which minimizes the energy increment in a homogeneous shear stress field given at infinity. This is a transient model between a single energy-minimizing hole and a regularly perforated plate, both numerically solved by a genetic optimization algorithm together with a fast and accurate fitness evaluation scheme using the complex-valued elastic potentials which are specifically arranged to incorporate a traction-free hole boundary. Here the scheme is further enhanced by a novel shape-encoding procedure through a conformal mapping of a *single* hole rather than *both holes simultaneously* as is done in standard practice. The optimized shapes appear to be slightly rounded elongated quadrangles aligned with the principal load axes. Compared to the single (square-like) optimal hole, they induce up to 12% less energy depending on the hole spacing. Qualitatively, it is also shown that the local stresses, computed along the optimal shapes as a less accurate by-product of the optimization, exhibit a tendency to be *piecewise constant* with no local concentration.

### 1. Introduction

Multiple closely spaced holes are widely employed in engineering design. Fulfilling technological functions, they weaken the structure and hence may substantially reduce its mechanical performance. This happens due to high local stresses and energy concentration induced by the holes in an applied external field. The resulting stress state of the structure depends on the holes' shapes, areas and mutual arrangement. Amongst these geometrical factors, the shapes are of less technological importance and can be used by designers to achieve a more favorable stress state of the construction.

Quantitatively, the state is assessed by any of three interrelated criteria:

- (A) the maximum of the von Mises stresses along the hole shapes;
- (B) the maximum of the squared tangential stress variations. In the ideal case of zero variations (a constant or piecewise constant stress distribution) no stress concentrations occur along the boundary;
- (C) the energy increment brought by the holes into a given outer stress field.

Minimization of A, B or C gives some optimal properties to the perforated plate. Here, we deal with the energy criterion C. The following considerations weigh in favor of our choice. First, for a finite number of holes, this increment is the zeroth-order approximation of the measurable effective moduli of an elastic perforated structure and hence has a clear physical meaning. The lesser the energy, the stiffer the plate. Second, the tangential stress constancy (criterion B) is the necessary condition of the energy

---

*Keywords:* plane elasticity problem, Kolosov–Muskhelishvili potentials, shape optimization, effective energy, extremal elastic structures, genetic algorithm.

minimum (criterion C) as shown by Banichuk [1977] through variation of the energy integral. In other words, the energy-minimizing holes simultaneously smooth the stress distribution. At the same time, the integral criterion C is computationally much easier than A and B, both of local nature.

Finally, there is the strong practical correlation between the criteria A and C. For a single hole under remote shear, it was semianalytically found in [Vigdergauz 2006] that the energy-minimizing hole provides almost the global minimum of the stresses (criterion A). Moreover, in the opposite case of uniform loads of the same sign, we proved analytically in [Vigdergauz 1976] that all three criteria are minimized for the same holes, called *equistress holes* (in accordance with criterion B). They are found by applying the equistress principle [Cherepanov 1974], which says that the tangential stresses along the optimal traction-free boundary are uniform. At a given number of holes this allows us to obtain the parametric equations of the equistress shapes depending on the ratio between the far loads and on a number of geometrical parameters which govern the mutual hole arrangement. We note in passing that Waldman et al. [2003] questioned this finding. Their assertion that "it turns out that Cherepanov's solution is for (two) holes that do not interact to any appreciable degree" is simply caused by confusing the parameters. Namely, the modulus of the elliptic integrals in Cherepanov's solution is specifically taken as  $1/2$ , while actually it varies between zero and one, thus covering any holes separation distance. In particular, with the modulus tending to one, the optimal holes come closer and closer together. Further, Waldman et al. [2003] misinterpreted our paper [Vigdergauz 1982] as dealing with two equistress holes in a plane. Actually, a distinctly different case of the equistress hole in a *half*-plane is considered there in an attempt to study the interaction between the hole and the traction-free edge. Nevertheless, the cited paper contains an informative variety of numerical results related to criterion B optimization, which we use later for reference.

Returning to criterion C we note that the increment divided by the total area of the holes depends only on the geometry. The corresponding shape optimization problem reads: *Given a uniform far-field loading, an area of two traction-free identical holes in a thin infinite elastic plate and their spacing, find, among all admissible continuous curves, the hole shape which minimizes the induced energy increment.*

For concreteness, we restrict discussion to only two interacting holes, though most derivations are easily generalized.

From the above it follows that this shape optimization problem is yet unsolved only for remote loads of opposite signs when the equistress principle is no longer valid, as explained in Section 3. In this case, numerical optimization required.

Any optimization process includes an iteration scheme and a repetitively used direct problem solver, both of great importance for converging to true optimum. Generally, the iteration process employs gradient or nongradient methods which perform directional and nondirectional searching, respectively. As in our previous papers [Vigdergauz 2001a; 2001b; 2006] we use here a nondirectional genetic optimization algorithm (GA). The feasibility of GA-based shape optimization in continuum mechanics has firstly been witnessed by Schoenauer et al. [1996]. The major advantage of this approach is that it explores the solution space by testing parameter combinations simultaneously to avoid local minima and requires no derivative information [Oszyczka 2001].

We couple GA with the direct problem solver based on the one-potential formulation given in [Vigdergauz 2001a] of the complex-valued Kolosov–Muskhelishvili (KM) functions [Muskhelishvili 1963]. The forward problem is then reduced to solving a system of linear algebraic equations where only the first unknown is needed for the energy evaluation of a given hole shape. The main difficulty here is evaluating

the shape integrals which enter into the system coefficients. Within the GA optimization, it induces the question of how to effectively encode an arbitrary hole shape. The serious disadvantage of the commonly used nodal points discretization is that the nodes simultaneously serve as design variables and as integration points. As a consequence, the number of nodes should be large enough (typically several tens or hundreds) for both adequate shape description and accurate integration. This impairs the convergence of the optimization process because it needlessly enlarges the problem size and hence raises the computation time.

Here we suggest an alternative approach which *separates* the design variables and the integration points. To this end, the fact is employed that the exterior of a unit circle can be conformally mapped holomorphically onto the exterior of any closed shape [Alfors 1979]. We use the first several coefficients of its Laurent expansion as the design variables while the integration is performed over a circle at fixed points independent of the optimization. This novelty drastically reduces the computational efforts and permits us to obtain detailed results at reasonable accuracy.

In contrast to common practice, neither the elastic domain nor the stress-strain equations are really transformed. The mapping is used for the pure geometrical purpose of encoding the searched shapes.

Our contribution is thus twofold: (i) a new, effective, and easily adaptive shape-decoding scheme for gradientless searching algorithms is proposed, and (ii) the energy-minimizing interacting holes in an elastic plane are numerically found on this basis.

Of course, the proposed scheme is not the only possible one. Good results have recently been obtained by Waldman et al. [2003]. They use the finite element analysis within a specific gradientless shape optimization method to identify the stress-constant holes (criterion B). In our opinion, both methods complement each other. Numerical examples show that the finite element method (FEM) gives the stresses with better accuracy, especially under a pure shear loading. The reason for this is explained in Section 7. On the other hand, the KM functions can easily tackle an infinite domain and hence are more suitable for the current purpose of minimizing the energy increment. It would thus be interesting to combine the direct FEM solver with the proposed shape encoding scheme within a gradientless searching to solve the stress minimization problem. However, this is beyond the scope of our paper.

Following is the outline of the rest of the paper. In Section 2 the two-dimensional boundary value elastostatic problem for a multiconnected infinite region is formulated in complex-variable terms for further references and the inverse shape identification problem is stated in detail. In Section 3 some closed-form identities are derived for assessing the future numerical results. The forward problem solver is described in Section 4 which is also concerned with the numerical validation of the proposed solver by comparison with alternatively obtained results available in literature. A key Section 5 presents the novel shape encoding scheme based on conformal mapping. Section 6 displays the GA framework specifically designed for our current purposes. In Section 7 numerical results are presented in detail and the capabilities of the scheme are tested, depending on the quantitative parameters involved. The paper ends with some concluding remarks in Section 8.

## 2. Basic relations in two-dimensional elastostatics

Consider the setup in Figure 1. Let a thin infinite plate be weakened by two identical holes, each of area  $F$ , symmetrically located on the  $X$ -axis of the complex plane  $E : z = x + iy$ . The hole boundary

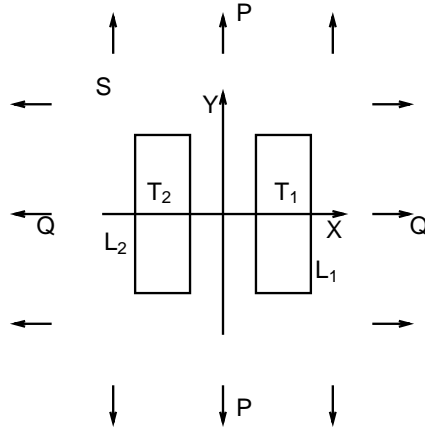


**Figure 1.** Schematic of the problem: an infinite plate with two identical holes under uniform stresses, the cases  $P = Q$  and  $P = -Q$  correspond to remote bulk and shear, respectively. The piecewise smooth hole shape is symmetric about the  $x$ -axis and may have a finite number of angular points.

$L = L_2 + L_1$  divides  $E$  into the isolated regions  $\{T_1, T_2 : T_1 + T_2 = T\}$  inside the holes and the outer connected region  $S = E - T$  occupied by a linearly elastic material with bulk and shear moduli  $K$  and  $\mu$ , respectively. The half-spacing  $d_0$  between the holes is measured as the minimal distance of the right hole to the  $y$ -axis:

$$d_0 = \min x : x + iy \equiv t \in L_1; \quad d_0 \geq 0. \tag{2.1}$$

Furthermore, let the plate be remotely loaded by uniform nontangential stresses:

$$\sigma_{xx}^\infty = P_0, \quad \sigma_{yy}^\infty = Q_0, \quad \sigma_{xy}^\infty = 0. \tag{2.2}$$

The cases  $P_0 = Q_0$  and  $P_0 = -Q_0$  correspond to remote bulk and shear, respectively. Both settings preserve twofold geometrical symmetry, by which the regions  $S$  and  $T$  go into themselves when rotating around the origin through the angle  $\pi$ .

The resulting stresses in  $S$  are governed by the biharmonic Airy function which, though useful as a theoretical tool, is numerically ineffective. Far more advantageous is the complex variable approach of replacing the Airy function with a pair of holomorphic functions  $\varphi_0(z), \psi_0(z), z \in S + L$  (the KM potentials [England 1971; Muskhelishvili 1963, Sections 47–51]) with the remote field asymptotics governed by (2.2):

$$\varphi_0(z) = B_0z + \varphi(z), \quad \psi_0(z) = \Gamma_0z + \psi(z) \quad \text{for } z \in S + L, \tag{2.3a}$$

$$\varphi(z) = \frac{2a_1}{z} + O(|z|^{-2}), \quad \psi(z) = \frac{2b_1}{z} + O(|z|^{-2}) \quad \text{as } z \rightarrow \infty, \tag{2.3b}$$

$$4B_0 = \text{Tr}\{\sigma^\infty\} = Q_0 + P_0, \quad 2\Gamma_0 = \text{Dev}\{\sigma^\infty\} = Q_0 - P_0, \quad \text{Im } B_0, \quad \text{Im } \Gamma_0 = 0. \tag{2.3c}$$

The leading asymptotic terms  $2a_1, 2b_1$  with the multiplier 2 are written thus for later convenience.

Due to the setup symmetry, the potentials  $\varphi(z)$ ,  $\psi(z)$  are uneven:

$$\varphi(-z) = -\varphi(z), \quad \psi(-z) = -\psi(z) \quad \text{for } z \in S + L, \quad (2.4)$$

and take conjugate values at complex conjugate points [Muskhelishvili 1963]:

$$\varphi(\bar{z}) = \overline{\varphi(z)}, \quad \psi(\bar{z}) = \overline{\psi(z)} \quad \text{for } z \in S + L. \quad (2.5)$$

With this in view, the following Laurent expansions are valid in  $S + L$  [Alfors 1979]:

$$\begin{aligned} \varphi(z) &= \sum_{k=1}^{\infty} a_k \left( \frac{1}{(z-c)^k} - \frac{(-1)^k}{(z+c)^k} \right), & \psi(z) &= \sum_{k=1}^{\infty} b_k \left( \frac{1}{(z-c)^k} - \frac{(-1)^k}{(z+c)^k} \right), \\ \operatorname{Im} a_k &= \operatorname{Im} b_k = 0 \quad \text{for } k = 1, 2, \dots, \end{aligned} \quad (2.6)$$

where  $c$  is a fixed point on the  $X$ -axis inside the hole  $T_1$  ( $\operatorname{Im} c = 0$ ,  $c > d_0$ ). In conformity with (2.3b), we have

$$\lim_{z \rightarrow \infty} z\varphi(z) = 2a_1, \quad \lim_{z \rightarrow \infty} z\psi(z) = 2b_1. \quad (2.7)$$

By residue theory [Alfors 1979], the first coefficients  $a_1$ ,  $b_1$  in (2.6) are equally expressed as

$$2a_1 = -\frac{1}{2\pi i} \int_L \varphi(t) dt, \quad 2b_1 = -\frac{1}{2\pi i} \int_L \psi(t) dt. \quad (2.8)$$

Dimensionally, they are proportional to the hole area  $F$  [Muskhelishvili 1963]

$$a_1 = \alpha_1 F, \quad b_1 = \beta_1 F, \quad (2.9)$$

where, in turn,  $F$  is given by the contour integral [Alfors 1979]

$$2F = \frac{1}{2i} \int_L \bar{t} dt = \frac{1}{i} \int_{L_j} \bar{t} dt \quad \text{for } j = 1, 2, \quad (2.10)$$

while

$$\frac{1}{2\pi i} \int_{L_j} t^n dt = 0, \quad \frac{1}{2\pi i} \int_{L_j} \frac{dt}{(t-z)^n} = \delta_{n,1} \quad \text{for } n = 0, 1, \dots, z \in L_j, j = 1, 2. \quad (2.11)$$

Here  $\delta$  is the Kronecker delta. All the integrals above are traversed counterclockwise.

For simplicity in further manipulations, suppose that the hole boundary  $L$  is traction-free:

$$\sigma_{\rho\rho}(t) = \sigma_{\rho\tau}(t) = 0 \quad \text{for all } t \in L, \quad (2.12)$$

where  $\sigma(t) = \{\sigma_{\rho\rho}, \sigma_{\tau\tau}, \sigma_{\rho\tau}\}$  represents the stress tensor in a local system of curvilinear orthogonal coordinates  $(\rho, \tau)$  at a point  $t \in L$ . With the KM potentials, (2.12) possesses the form

$$\overline{\varphi(t)} + \bar{t}\varphi'(t) + \psi(t) = -2B_0\bar{t} - \Gamma_0 t + C_j \quad \text{for } t \in L_j, j = 1, 2. \quad (2.13)$$

Here the  $C_j$  are free complex-valued constants not affecting the stress field. Identity (2.13) forms a boundary value problem in the holomorphic functions  $\varphi(z)$ ,  $\psi(z)$  with first-order vanishing conditions (2.3) at infinity. For a proper choice of the constants  $C_j$ , this problem is uniquely solvable [Muskhelishvili 1963] in a broad class  $\{L\}$  of continuous hole shapes. The solved functions  $\varphi(z)$ ,  $\psi(z)$  completely describe

the hole-induced distortion of the homogeneous field (2.2). Remarkably, the Cartesian displacements  $u_x(t), u_y(t)$  of the boundary points  $t \in L$  are expressed only through  $\varphi(z)$  [Vigdergauz 2001a]:

$$u_x(t) + iu_y(t) = \left(\frac{1}{K} + \frac{1}{\mu}\right)(B_0t + \varphi(t)) \quad \text{for } t \in L, \tag{2.14}$$

as is the nonzero stress component  $\sigma_{\tau\tau}(t)$  [Muskhelishvili 1963]:

$$\sigma_{\tau\tau}(t) = 4B_0 + 4 \operatorname{Re} \varphi'(t) \quad \text{for } t \in L. \tag{2.15}$$

Combining (2.14) and (2.15), we arrive at an interesting identity which holds only at a traction-free hole boundary

$$\sigma_{\tau\tau}(t) = 4\left(\frac{1}{K} + \frac{1}{\mu}\right)^{-1} \operatorname{Re}(u'_x(t) + iu'_y(t)). \tag{2.16}$$

Application of the maximum principle to the harmonic function  $\operatorname{Re} \varphi_0(z)$  provides (after some algebra) the interesting lower bound [Vigdergauz 1976]

$$\max |\operatorname{Re} \varphi_0(t)| \geq |\varphi_0(\infty)| \implies \mathcal{M} \equiv \max |\sigma_{\tau\tau}(t)| \geq 4|B_0| \quad \text{for } t \in L, \tag{2.17}$$

which turns out to be attainable (see the next section). At a free boundary  $|\sigma_{\tau\tau}(t)|$  coincides with the von Mises stresses.

The stresses at any point inside  $S$  are also expressed in  $\varphi(z), \psi(z)$ . We omit the corresponding formulae to save room.

At a given loading, the potentials  $\varphi(z), \psi(z)$  and hence the stress distortion depend only on the hole shapes and their mutual location defined by the dimensionless parameter  $\lambda = d_0\sqrt{\pi/F}$  (the multiplier  $\pi$  serves for convenient comparison with the literature data where a unit circle with  $F = \pi$  is usually considered). This one-parameter dependence brings up the optimization problem:

*To find the hole shapes that minimize the stress distortion as measured through the induced strain energy increment  $\Delta W$  divided by the total hole area  $2F$ .*

$$\Delta W(B_0, \Gamma_0, \lambda, L) \xrightarrow{\{L\}} \min(B_0, \Gamma_0, \lambda), \tag{2.18}$$

The lesser the increment, the stiffer the plate weakened by the holes. Mathematically,  $\Delta W$  takes the form of the first-order approximation to the effective moduli of a regularly perforated plate when the volume fraction of the hole is vanishingly small. Due to its averaging nature, the energy increment involves only the first terms (2.9) of the expansion (2.6) [Jasiuk 1995; Vigdergauz 2001a]

$$\Delta W = 8\pi(2\Gamma_0\alpha_1 + B_0\beta_1)\left(\frac{1}{K} + \frac{1}{\mu}\right). \tag{2.19}$$

Nevertheless,  $\Delta W$  can be extracted and optimized only from the full-size solution of the problem (2.13). The optimization strategy depends on whether the ratio  $|\operatorname{Dev}\{\sigma^\infty\} / \operatorname{Tr}\{\sigma^\infty\}|$  in (2.3c) is less than 1. Physically, this ratio measures the far-field anisotropy.

### 3. Bulk load: analytical relations for the equistress shapes

When the deviatoric part of  $\sigma^\infty$  is no larger than its trace

$$|\delta_0| \leq 1; \quad \delta_0 \equiv \frac{\text{Dev}\{\sigma^\infty\}}{\text{Tr}\{\sigma^\infty\}} = \frac{Q_0 - P_0}{Q_0 + P_0} = \frac{\Gamma_0}{2B_0}, \quad (3.1)$$

or, equivalently, the far loads are of the same sign, the inverse problem (2.18) admits a remarkable solution dating back to the pioneering work by Cherepanov [1974]. Namely, if  $\varphi(z)$  is identical to zero,

$$\varphi(z) \equiv 0, \quad z \in S + L, \quad (3.2)$$

then the traction-free condition (2.13) goes into the resolving equation for  $\psi(z)$  :

$$\psi(t) = -2B_0\bar{t} - \Gamma_0 t + C_j \quad \text{for } t \in L_j, \quad j = 1, 2. \quad (3.3)$$

Actually, identity (3.3) presents the *inverse* problem of finding the shapes which bear the given values of a holomorphic function vanishing at infinity. With (3.1) and, possibly, nonzero constants  $C_j$ , this problem is proven to be uniquely solvable under the necessary condition

$$\|\Gamma_0\| \leq 2\|B_0\|. \quad (3.4)$$

Indeed, differentiating (3.3) with respect to  $t$  and taking the real parts of both sides we arrive at

$$\text{Re } \psi'(t) = -\Gamma_0 - 2B_0 \text{Re } \frac{\partial \bar{t}}{\partial t} \quad \text{for } t \in L_j, \quad j = 1, 2, \quad (3.5)$$

where the harmonic function  $u(x, y) \equiv \text{Re } \psi'(t)$  vanishes at infinity. The Mean Value theorem [Alfors 1979] implies that  $u(x, y)$  has at least one zero on  $L$ , so that

$$\Gamma_0 = -2B_0 \text{Re } \frac{\partial \bar{t}_0}{\partial t_0} \quad \text{for } t_0 \in L. \quad (3.6)$$

The well-known inequality  $\|\partial \bar{t}/\partial t\| \leq 1$  [Alfors 1979] makes (3.6) equivalent to (3.4). The corresponding function  $\psi(z)$  is further referred to as the domain characteristic function  $\Omega_0(z) \equiv \psi(z)$  [Vigdergauz 1988]. The resultant holes exist for any mutual arrangement, up to their touching. They simultaneously possess some analytically derived optimal properties:

- First, substitution of (3.2) into (2.15) shows that the stress distribution along the hole shapes (3.3) is *uniform*:

$$\sigma_{\tau\tau}(t) = \text{Const} = 4B_0 \quad \text{for } t \in L, \quad (3.7)$$

with no local concentration potentially harmful for the plate strength. Because of (3.7) these are called equistress or equistrength holes [Cherepanov 1974].

- Second, the equistress condition (3.2) saturates inequality (2.17), thus giving the global minimum to the maximum von Mises stresses over all possible hole shapes:

$$\min_{\{L\}} \max_{t \in L} |\sigma_{\tau\tau}(t)| = \min_{\{L\}} \max_{t \in L} \mathcal{M} = 4B_0 \quad \text{for } \delta_0 \leq 1. \quad (3.8)$$

• Finally, substituting (3.3) into (2.19) and making use of (2.10), (2.11) we arrive at the energy increment value

$$\Delta W = 4B^2 \left( \frac{1}{K} + \frac{1}{\mu} \right), \tag{3.9}$$

which again turns out to be the global minimum [Gibiansky and Cherkaev 1984].

All three criteria (3.7)–(3.9) are independent of the far stresses deviator  $\Gamma_0$  and the relative distance between the holes, while the equistress shapes do depend on both, as dictated by (3.3). Particularly, the equistress *isolated* hole is simply an ellipse [Cherepanov 1974] with eccentricity  $\delta_0$  elongated along the far field eigendirection of the maximum  $|P_0|, |Q_0|$ . Some specific arrangements of the optimal *interacting* holes are found in [Cherepanov 1974; Vigdergauz 1976; Grabovsky and Kohn 1995; Vigdergauz 1996]. Commonly, the equistress shapes are smooth with no angular points.

Pairs of equistress holes are numerically reproduced in [Waldman et al. 2003]. As compared to the analytical shape equation derived in [Cherepanov 1974] (and generalized as explained in the Introduction), these findings bring no novelty to the equistress solutions but they help to verify the proposed FEM-based stress optimization scheme.

With the properties we have shown, we are now in a position to derive a guiding inequality for  $\Delta W$  *outside* the interval (3.1). Indeed, let a plate with equistress holes be subject to an arbitrary far load:  $P, Q$  with  $4B = P + Q, 2\Gamma = Q - P$ . Integration of the traction-free condition (2.13) over  $L$  separately with respect to  $dt$  and  $d\bar{t}$  gives:

$$\int_L \overline{\varphi(t)} dt + \int_L \bar{i} \varphi'(t) dt + \int_L \psi(t) dt = -2B \int_L \bar{i} dt - \Gamma \int_L t dt + C_1 \int_{L_1} dt + C_2 \int_{L_2} dt, \tag{3.10a}$$

$$\int_L \overline{\varphi(t)} d\bar{t} + \int_L \bar{i} \varphi'(t) d\bar{t} + \int_L \psi(t) d\bar{t} = -2B \int_L \bar{i} d\bar{t} - \Gamma \int_L t d\bar{t} + C_1 \int_{L_1} d\bar{t} + C_2 \int_{L_2} d\bar{t}. \tag{3.10b}$$

Consider the first identity (3.10a). With (2.10) and (2.11), all integrals, excepting the first two, are taken in the form independent of the holes shapes. For the equistress boundaries, the remaining integrals can also be written explicitly. To this end, separately differentiating the characteristic Equation (3.3) with respect to  $t$  and  $\bar{t}$ ,

$$dt = (-2B_0)^{-1} (\overline{\Omega'_0(t)} + \Gamma_0) d\bar{t}; \quad B_0 \neq 0, \tag{3.11a}$$

$$d\bar{t} = (-2B_0)^{-1} (\Omega'_0(t) + \Gamma_0) dt, \tag{3.11b}$$

we have

$$\int_L \overline{\varphi(t)} dt = (-2B_0)^{-1} \int_L \overline{\varphi(t)} (\overline{\Omega'_0(t)} + \Gamma_0) d\bar{t}. \tag{3.12}$$

The first integral on the right-hand side of (3.12) is the conjugate value of the residue at infinity of the holomorphic function  $\varphi(z)\Omega'_0(z)$ . It vanishes because, in view of (2.3b), we have  $\varphi(z)\Omega_0(z)' = O(|z|^{-3})$  as  $z \rightarrow \infty$ . Finally, from (2.8) we get

$$\int_L \overline{\varphi(t)} dt = (-2B_0)^{-1} \Gamma_0 \int_L \overline{\varphi(t)} d\bar{t} = 2\pi i \frac{\Gamma_0}{B_0} a_1 = 4\pi i \delta_0 a_1. \tag{3.13}$$

Similarly, in view of (3.11b), the remaining integral in (3.10a) takes the form

$$\int_L \bar{t} \varphi'(t) dt = - \int_L \varphi(t) d\bar{t} = 2\pi i \frac{\Gamma_0}{B_0} a_1 = 4\pi i \delta_0 a_1. \quad (3.14)$$

The second identity (3.10b) is treated in same manner so that (3.10) goes into a  $(2 \times 2)$  system of linear algebraic equations in the unknown residues  $a_1, b_1$  of the potentials  $\varphi(z), \psi(z)$ :

$$2\delta_0 a_1 + b_1 = \frac{2B}{\pi} F, \quad (1 + \delta_0^2) a_1 + \delta_0 b_1 = \frac{\Gamma}{\pi} F, \quad (3.15)$$

with the solution

$$a_1 = \frac{\Gamma - 2B\delta_0}{\pi(1 - \delta_0^2)} F, \quad b_1 = \frac{B(1 + \delta_0^2) - \Gamma\delta_0}{\pi(1 - \delta_0^2)} 2F, \quad (3.16)$$

substitution of which into (2.19) yields

$$\Delta W = \frac{4(B^2(1 + \delta_0^2) + \Gamma^2 - 3\delta_0 B\Gamma)}{1 - \delta_0^2} \left( \frac{1}{K} + \frac{1}{\mu} \right). \quad (3.17)$$

Of course, (3.17) returns to (3.9) for the initial load parameters:  $B = B_0, \Gamma = \Gamma_0$ .

Again, this equistress relation involves neither the number of holes nor their arrangement and hence may serve as a geometry-independent upper assessment of  $\min \Delta W$  under predominating shear when the equistress necessary condition (3.1) is not valid or, equivalently, the far loads are of opposite signs. In particular, taken at the bulk-type initial load ( $\Gamma_0, \delta_0 = 0$ ), the equistress holes induce the following increment under pure shear ( $B = 0, \Gamma = 1$ ):

$$\Delta W(0, 1, \lambda, L) = 4 \left( \frac{1}{K} + \frac{1}{\mu} \right), \quad (3.18)$$

which is larger than the global minimum:

$$\Delta W(0, 1, \lambda, L) \approx 3.71449 \left( \frac{1}{K} + \frac{1}{\mu} \right), \quad (3.19)$$

known in the limiting case  $\lambda \rightarrow \infty$  of a single hole and attained at the square-like shape [Vigdergauz and Cherkayev 1986]. Though not sharp, the upper bound (3.18) is useful in assessing numerical results (Section 7).

#### 4. Pure shear: fast direct solver

In contrast, a shear-dominated remote loading (outside interval (3.1)) admits no closed-form optimal solution and hence must be treated numerically. Any numerical optimization involves, in one way or another, repeated solving of the direct problem (2.13), (2.3). The more accurate and faster the direct solver is, the better the optimization scheme works as a whole. Besides, the solver should match stringent requirements of the computer memory, speed and computational stability.

Particularly relevant here is the approach first proposed and implemented by the author for a single hole [Vigdergauz 2001a;2006] and for a regularly perforated plate [Vigdergauz 2001b]. The key idea is to solve the KM potentials in *tandem rather than in parallel*. Since the basic features of the approach are

covered in the above-referenced papers, here we specifically focus on its application to a multiconnected region.

Identity (2.13) resolved for  $\psi(t)$  and differentiated with respect to  $t$

$$-\psi'(t) = 2 \frac{\partial \bar{t}}{\partial t} \operatorname{Re} \varphi'(t) + \bar{t} \varphi''(t) + 2B_0 \frac{\partial \bar{t}}{\partial t} + \Gamma_0, \quad t \in L, \tag{4.1}$$

implies that the right hand-side of (4.1) is the boundary value of a function holomorphic in  $S$  and vanishing at infinity. Then the Cauchy-type integral

$$\int_{L_1+L_2} \frac{2 \frac{\partial \bar{t}}{\partial t} \operatorname{Re} \varphi'(t) + \bar{t} \varphi''(t) + 2B_0 \frac{\partial \bar{t}}{\partial t} + \Gamma_0}{t - z} dt \tag{4.2}$$

is identically zero at any point  $z \in T$  [Muskhelishvili 1963]. The symmetry relations (2.4) reduce the integration path in (4.2) to only  $L_1$ . With (2.11), some algebra yields

$$2 \int_{L_1} \operatorname{Re} \varphi'(t) \rho_0(t, z) d\bar{t} + \int_{L_1} \bar{t} \varphi''(t) \rho_0(t, z) dt = -4B_0 \int_{L_1} \rho_0(t, z) d\bar{t} - 2\Gamma_0, \tag{4.3}$$

$$\rho_0(t, z) \equiv \frac{1}{t - z} + \frac{1}{t + z} \quad \text{for } z \in T.$$

Cauchy-type integrals in (4.3) are holomorphic functions of  $z$  in the hole’s region  $T$ . Consequently, this identity holds everywhere in  $T$  if and only if it holds for all derivatives with respect to  $z$  at a given point  $z = c \in T_1$  [Muskhelishvili 1963]:

$$2 \int_{L_1} \operatorname{Re} \varphi'(t) \rho_k(t, c) d\bar{t} + \int_{L_1} \bar{t} \varphi''(t) \rho_k(t, c) dt = -4B_0 \int_{L_1} \rho_k(t, c) d\bar{t} - 2\Gamma_0 \delta_{k,0}, \tag{4.4}$$

$$\rho_k(t, c) \equiv \frac{1}{k!} \frac{\partial^k \rho_0(t, z)}{\partial z^k} \Big|_{z=c} = \frac{1}{(t - c)^{k+1}} + \frac{(-1)^k}{(t + c)^{k+1}} \quad \text{for } k = 0, 1, 2, \dots$$

As one would expect, the Laurent expansion (2.6) for  $\varphi(z)$  and its derivatives similarly involve the kernels  $\rho_k(z, c)$ . Substitution of them into the left-hand side of (4.4) gives an infinite system of linear algebraic equations in the desired unknowns  $\{a_1, a_2, \dots\}$  from (2.6) with the matrix  $A = \{A_{kl}\}$ :

$$A_{kl} = 2l \int_{L_1} \operatorname{Re}(\rho_{l+1}(t, c)) \rho_k(t, c) d\bar{t} + l(l + 1) \int_{L_1} \bar{t} \rho_{l+2}(t, c) \rho_k(t, c) dt. \tag{4.5}$$

Due to the adopted symmetry, the system is purely real. For computation purposes it is necessarily truncated to a finite order  $N$ . This is all the more relevant since the first coefficient  $a_1$  alone appears in the energy increment for pure shear. As mentioned in Section 2, the displacements (2.14) and the tangential stresses (2.15) along a free boundary are also expressed only through  $\varphi(z)$ . In other words, the second potential  $\psi(z)$  is not involved in the current solution process, thus halving the computational efforts as compared to more traditional approaches. This feature is particularly appealing for repetitive use within evolutionary optimization algorithms.

For a circular hole  $L_1 : |t - c| = 1$

$$\bar{t} = c + \frac{1}{t - c}, \quad \frac{\partial \bar{t}}{\partial t} = -\frac{1}{(t - c)^2} \quad \text{for } t \in L_1, \tag{4.6}$$

the integrals in (4.5) are expressed analytically. Indeed, with (4.6), the conjugates  $\overline{\rho_k(t, c)}$  can be expanded around the point  $t = c$  as

$$\overline{\rho_k(t, c)} = \frac{1}{(\bar{t} - c)^{k+1}} + \frac{(-1)^k}{(\bar{t} + c)^{k+1}} = (t - c)^{k+1} + \frac{(-1)^k}{2c} \sum_{j=0}^{\infty} \binom{-m}{j} \left(\frac{t - c}{2c}\right)^j, \quad (4.7)$$

where

$$\binom{-m}{j} = (-1)^j \frac{(m + j)!}{m! j!}.$$

The series (4.7) converges absolutely since  $2c > 1$ . Substituting (4.6) and (4.7) into (4.5) and computing the integrand's residue at the isolated pole  $z = a$  we obtain the similar series for  $A_{kl}$  and, when necessary, for the bulk-related right-hand side (4.4) of the system. The resultant expressions are not displayed here to save room.

It is interesting to verify the derived formulae by comparing the results against alternatively obtained solutions of the boundary value problem (2.13). The literature suggest various approaches to find the stress distribution along two interacting circular holes under remote loading. In parallel with rapid expansion in computer capabilities, the numerical schemes progressed from a closed-form solution with infinite sums in the bipolar coordinates [Ling 1948] and the alternative iterations [Ting et al. 1999] to the advanced FE analysis [Waldman et al. 2003] and to the highly accurate solution of the Sherman-type integral equation [Helsing and Jonsson 2000]. Tables 1 and 2 compare literature data against our results

		[Ting et al. 1999]	[Helsing and Jonsson 2000]	Present
$x$ -axial tension ( $P = 1, Q = 0$ )	Max	2.611		2.61038805
	Min	-0.918		-0.91768252
$y$ -axial tension ( $P = 0, Q = 1$ )	Max	6.107	6.106040764542	6.10604077
	Min	-0.962		-0.96154890

**Table 1.** Maximum and minimum tangential stresses (2.15) for two equal circular holes aligned with the  $x$ -axis at  $\lambda = 0.2$ .

$\lambda$	[Ling 1948]	[Waldman et al. 2003]	Present	$\lambda$	[Ling 1948]	[Waldman et al. 2003]	Present
0.0200	—	—	12.475899	0.5000	2.887	2.906	2.8874965
0.2101	—	3.955	3.9153632	1.0000	2.411	2.426	2.4108275
0.2500	—	3.682	3.6561422	2.0000	2.155	2.172	2.1545912
0.3500	—	3.259	3.2374789	4.0000	2.049	—	2.0488101
0.4568	—	2.990	2.9684777	7.0000	2.018	—	2.0177007

**Table 2.** Maximum tangential stresses (2.15) for two equal circular holes aligned with the  $x$ -axis under biaxial loading  $B_0 = 1, \Gamma_0 = 0$  as a function of  $\lambda$ . The relative error of approximation. 1% in [Waldman et al. 2003] can be attributed to taking a finite region instead of an infinite plate.

obtained at  $N = 30$  for different load modes and separation distance between holes. The values show close agreement, which should be even better for the less sensitive energy increment.

**5. The design variables: an efficient shape parameterization**

In contrast to circles, general hole shapes must be treated numerically. Usually, they are presented by equally spaced nodal points whose role is twofold. First, they form a discretization set to compute the integrals (4.5). Second, they serve as optimized design variables. However, this results in a contradiction in the goals, inasmuch as the number of nodes should be sufficiently large to perform an accurate integration but rather small to carry out an efficient optimization over the pool of shapes. In [Vigdergauz 2006] we proposed a much more economic alternative which separates the design variables and the integration points by using for the first purpose the finite-term conformal mapping of a centrally located unit circle  $\gamma$  onto the hole shape  $L_1$ . At a given normalized distance  $\lambda$  we have

$$t \in L_1 : t = c + \omega(\xi), \quad \omega(\xi) \equiv \xi + \sum_{m=1}^M d_m \xi^{-m}, \tag{5.1a}$$

$$F = \pi \left( 1 - \sum_{k=1}^K k d_k^2 \right), \quad (\xi = e^{i\vartheta} \in \gamma : |\xi| = 1), \tag{5.1b}$$

$$dt = i \omega'(\xi) \xi d\vartheta, \quad d\bar{t} = i \overline{\omega'(\xi)} \xi^{-1} d\vartheta, \tag{5.1c}$$

where the contour displacement  $c$  is defined in conformity with (2.1) as

$$c = -\lambda \sqrt{F/\pi} \min_t \operatorname{Re}(\omega(t)). \tag{5.2}$$

Because of the setup symmetry,  $\{d_m\}$  are real. As design variables, the mapping coefficients offer substantial numerical advantages enumerated in [Vigdergauz 2006]. For clarity, we display them here:

- (A) They are "naturally" ordered, in the sense that the higher the coefficient, the lesser its global impact on the inclusion shape. This means that even a small number of the first coefficients form a practically representative searching pool—in contrast to the nodal points.
- (B) Each mapping coefficient falls into the successively narrowed interval

$$-\frac{1}{\sqrt{m}} \leq d_m \leq \frac{1}{\sqrt{m}}, \quad m = 1, 2, \dots, \tag{5.3}$$

as it follows from the nonnegativeness of the area  $F$  inside  $L_1$  [Alfors 1979].

- (C) With (5.1c), the path  $L_1$  in (4.5) is transformed into the circle  $\gamma$  where the discrete points for numerical evaluation of the integrals can be taken in the irreducible interval  $[0, \pi]$  independently of the design variables  $\{d_m\}$ . For simplifying further computations we use a trapezoidal rule at  $N_{int}$  equal subintervals  $[n\pi/(N_{int}); (n + 1)\pi/N_{int}]$ ,  $n = 0, 1, \dots, N_{int} - 1$  which remain unchanged during the optimization.

- (D) Specifically, for interacting holes, the hole displacement  $a$  is explicitly expressed by (5.2).

Items (B) and (D) are hard to realize in a more traditional approach when the exterior of *all* holes is *simultaneously* mapped onto the plane minus the same number of circles.

We are in a position to verify the proposed approach for noncircular holes. The relevant comparison here is with the stress constancy (3.7) of the analytically known equistress shapes. At  $\lambda = 0.3$  the solver gives, after term-by-term differentiation, the stress distribution oscillating around the true value with the maximum relative deviation of 0.9% located along the interacting parts of the holes. However, for rectangle-like shapes the stress computations get worse drastically, because this leads to a very unfavorable situation. The first KM potential  $\varphi(z)$  is presented through the polar angle  $\vartheta$ , small increments of which lead to large increments along the straight line portions of the curves. With term-by-term differentiation, this manifests itself in very large stress oscillations which are further amplified by the fact that all the Laurent coefficients  $a_k$  but the first one remain outside the energy optimization. For a single hole this was first reported in [Cherkaev et al. 1998]. In other words, the one-potential scheme, especially structured for the energy assessment, is ineffective (in its current form) in computing the stresses along quadrangle-like holes, be it at  $M = 5$  or  $M = 100$  first mapping terms. Here, another stress solver should be used for optimization. Exclusively for illustration purposes, we will once again consider the local stresses at the end of Section 7.

## 6. Outline of the genetic algorithm

The optimization problem (2.18) typically has many local minima, and this fact precludes the use of gradient-based descent methods. An integer-encoded simple GA was chosen as the global shape optimization approach in the previous author's papers and in the present work.

The GA operates by constructing sets of candidate shapes and solving the forward problem for each. The design variables  $d_m$ ,  $m = \overline{(1, M)}$ , are encoded using a discrete 16-bit procedure when each coefficient  $d_m$  is approximated in view of (5.3) only by  $2^{16} - 1$  separate values in the continuous search space  $[-1/\sqrt{m}, 1/\sqrt{m}]$ . These values are decoded from a randomly generated integer  $p \in [-2^{15}, 2^{15}]$  as  $d_m = p/2^{15}/\sqrt{m}$ . The genes for different coefficients are concatenated into a  $16N$  binary chromosome that encodes a shape to be evaluated with the proposed approach. A randomly generated chromosome population of constant size is subject to bitwise crossover and mutations [Osyczka 2001] to produce the next generation. Then the process is repeated. This mimics the natural process where better members of a population tend to outperform others in the long run. In our situation, "better" means a lower fitness value. When the heuristic probability levels of genetic operations are adjusted correctly, they tend to bias towards better individuals in the population so that better genes are passed down to offspring. To enhance this effect, the best chromosome(s) from one generation are passed, unchanged, to the next (the *elitism* option). So the generations evolve, and if the optimization process is successful, the shapes in each generation are better, in a broad sense, than those in the previous one.

The stopping criterion is a problematic issue in GA, as there no practical means to assess the actual error in real applications. Instead, the optimization is stopped after the first  $N_{iter}$  iterations — in the belief that the process really converges. However, at specific stochastic combinations, GAs may become "embedded" far from the global optimum. This is prevented by multiple GA runs performed in the current work for each given problem. Practically,  $N_{iter}$  is chosen so that the optimization criterion remains unchanged in successive iterations well before reaching this limit.

In contrast to many other applications, here we have an opportunity to calibrate the GA heuristic parameters by numerically reproducing the optimal equistress shapes with the known global minimum

$\lambda$	$M = 3$	$M = 5$	$M = 7$	$M = 9$
0.01	$1.22 \times 10^{-2}$	$2.96 \times 10^{-3}$	$8.18 \times 10^{-4}$	$2.33 \times 10^{-4}$
0.25	$5.69 \times 10^{-3}$	$2.21 \times 10^{-4}$	$7.76 \times 10^{-5}$	$4.60 \times 10^{-5}$
0.50	$1.39 \times 10^{-3}$	$9.28 \times 10^{-5}$	$1.94 \times 10^{-5}$	$1.94 \times 10^{-5}$
1.0	$7.15 \times 10^{-5}$	$1.42 \times 10^{-5}$	$1.42 \times 10^{-5}$	$1.42 \times 10^{-5}$
2.0	$3.67 \times 10^{-6}$	$3.66 \times 10^{-6}$	$3.66 \times 10^{-6}$	$3.66 \times 10^{-6}$

**Table 3.** Relative deviations of the energy increment  $\Delta W$  from the exact value (3.9) for two holes under the bulk type loading  $P = Q = 1$  (equistress shapes) versus the number  $M$  of the mapping terms and the normalized distance  $\lambda$ .

(3.9). The results are grouped in Table 3 as a function of the distance  $\lambda$  and on the number  $M$  of the mapping coefficients.

In practice, each genetic operator has a lot of various modifications advanced in the literature for different applied purposes. However, a relatively small number  $M$  of required design variables permits a fairly simple GA configuration as detailed in Table 4. A typical convergence characteristic for the GA scheme is shown in Figure 2.

## 7. Numerical results

The GA-based simulations aim to numerically solve the optimization problem (2.18) in the representative interval of the normalized parameter  $\lambda$ . The proximity to the true minimum values can be only evaluated through the internal convergence of the results for successively increasing mapping size  $M$  of the problem

GA Parameter	Parameter value(s)
Gene	Integer $[-32767; 32767]$
Individual	Interface shape
Population size	800
Number of genes	up to 9
Initial population	800 random individuals
Selection	Tournament
Elitism	Four best individuals
Crossover	1-point
Crossover rate	0.90
Creep mutation	By randomly changing a bit
Creep mutation rate	0.35
Jump mutation	By adding a random integer, typically in the range $[-4; 4]$
Jump mutation rate	0.35
Stopping criterion	After 1200 iterations
Resolving system size	24
Number of integration points	720 (in the interval $[0, \pi]$ )

**Table 4.** GA operator types, their probability rates and related parameters typically used in further optimizations.

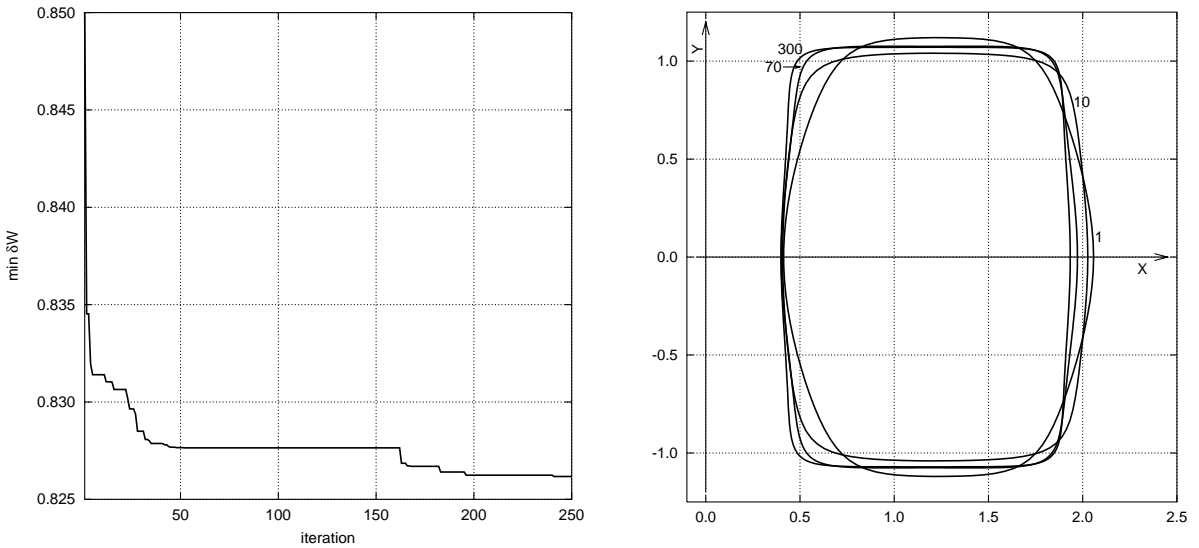


**Figure 2.** Hole shape identification: progress of a typical genetic optimization run.

as presented in Figure 3 and 4. For convenience, the increment is normalized by its value (3.18) for a circular hole under pure shear. It is seen that the approximants converge remarkably fast for any  $\lambda$ .

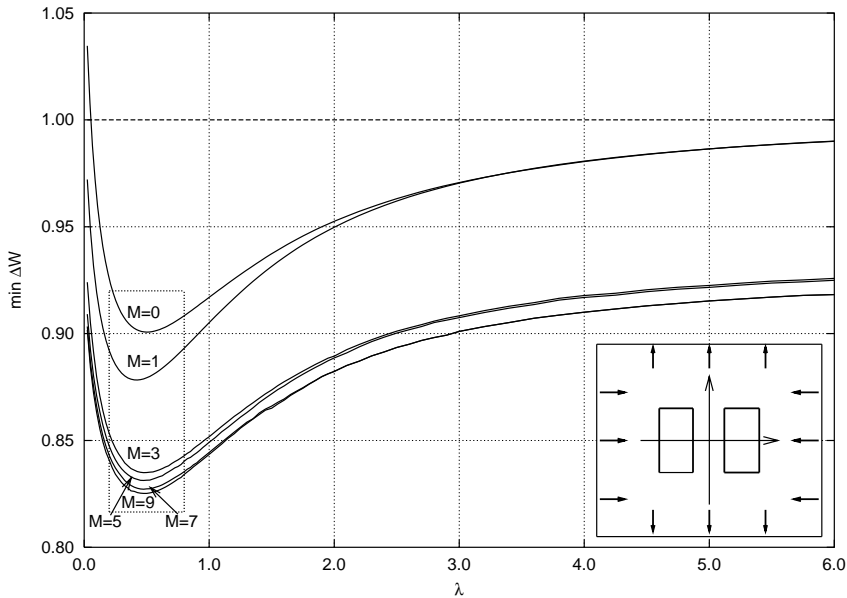


**Figure 3.** Minimum of  $\Delta W$  as a function of the distance  $\lambda$  as a function of the problem mapping size  $M$  beginning with a circle ( $M = 0$ ). The values are normalized by the equestress-related energy increment (3.18) (the dashed line) added here for comparison. The inset recalls the problem schematic. An enlarged view of the dotted rectangular is given in Figure 4.

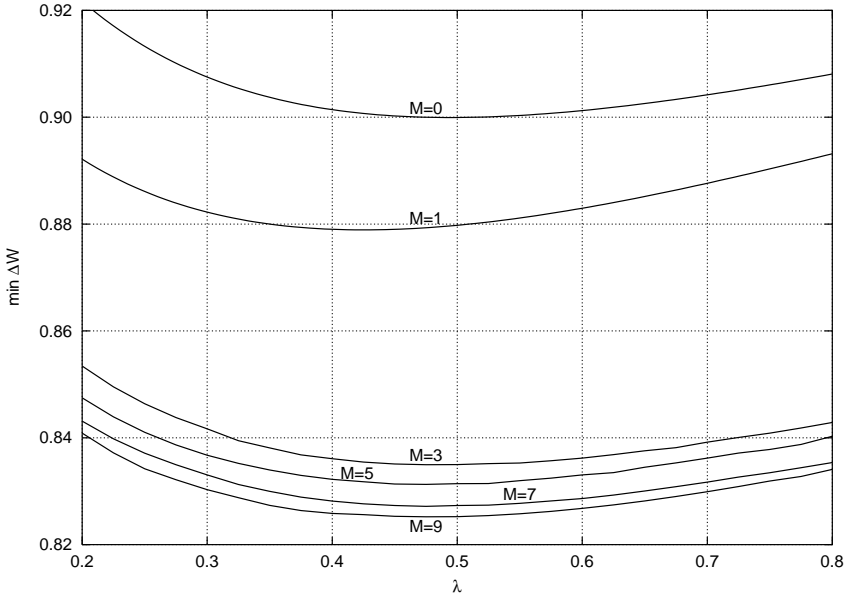


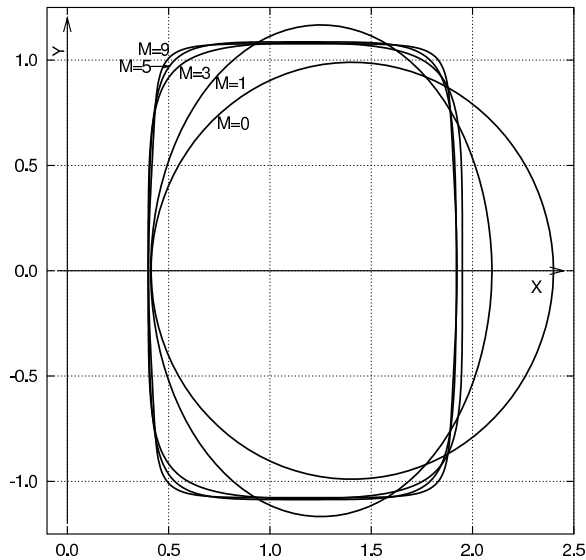
**Figure 4.** Enlarged fragment of Figure 3 around the global minima of  $\min \Delta W$  at  $\lambda \approx 0.45$ .

In the limiting case of a single hole ( $\lambda \rightarrow \infty$ ) the curves tend asymptotically to either the global minimum (3.19) for  $M \geq 3$  or to the bound (3.18) when the given  $(M + 1)$ -fold symmetry ( $M \leq 2$ ) allows for only the equistress circle instead of the truly optimal square-like shape.

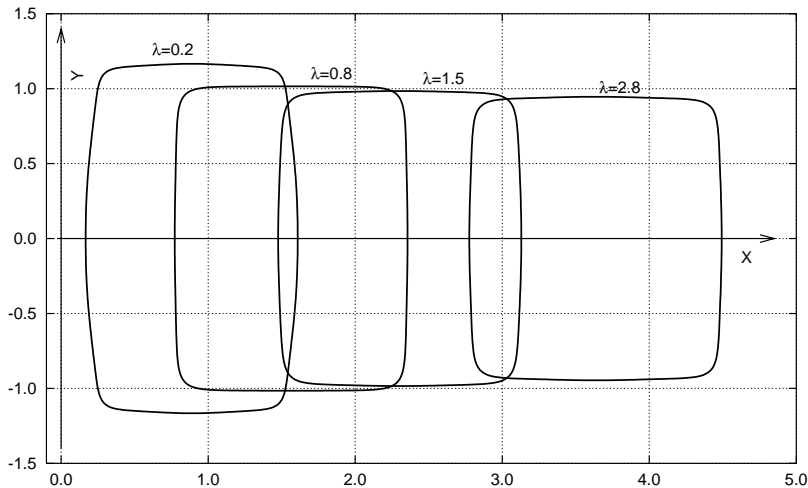
The most remarkable finding is that the shear-related optimized energy depends on the separation distance  $\lambda$  between the holes attaining the minimum at  $\lambda_{\min} \approx 0.45$ . In contrast to equistress holes, whose mutual arrangement has no impact on the induced energy, shear-optimal shapes exhibit a significant collective effect, conjectured and qualitatively explained in [Cherkaev n.d.]. Interaction of the simplest circular holes gives only 3.3% less energy at  $\lambda_{\min}$  than the optimal isolated square-like hole. More markedly, the optimized shapes conserve  $\approx 12\%$  of the perturbed energy for  $M = 9$ . This percentage consists of two quite unequal parts:  $12\% = 10.7\% + 1.3\%$ ; the dominating one relates to the first three coefficients while the contribution of the rest is much less. It is pictorially explained by

Figure 5 which shows the optimal shape evolution against the number  $M$  of mapping terms beginning with a circle ( $M = 0$ ). One can see that the quadrangle-like optimal shape is formed already at  $M = 3$  whereas the higher coefficients only flatten its sides and sharpen the angles. Such local improvements have less effect on the integral-type energy criterion. The analogy with the single optimal hole [Vigdergauz and Cherkayev 1986] suggests that the appearing angular points of the hole shape bring no singularities in the tangential stress distribution.

Figure 6 exemplifies the shape elongation as a function of the distance  $\lambda$  as resulting from the holes interaction. We note in parallel that the square-like single optimal hole also transforms into a rectangle as a function of a nonzero trace component in the remote shear-dominating load  $-1 < Q_0/P_0 < 0$ . Both elongations present the optimal response in the absence of the setup square symmetry caused by either the holes' location or the applied load. A marked feature of the optimal shapes is that they are vertically symmetric. In other words, the even coefficients  $d_m, m = 2, 4, \dots$  are invariably optimized to zero values.



**Figure 5.** Evolution of the energy-minimizing hole with the number of the mapping terms  $M$  at the distance  $\lambda = 0.4$ .



**Figure 6.** Evolution of the energy-minimizing hole with the distance  $\lambda$  at  $M = 9$ .

This is in contrast to the horizontal symmetry of the holes as predefined by taking only real values of  $d_k$ ,  $k = 0, 1, 2 \dots$  before the optimization process.

Table 5 presents the edge separation ratio  $\lambda/h$  introduced in [Waldman et al. 2003] (here  $h$  is the half height of the quadrangle) for the optimal shapes at  $M = 9$  for different values of  $\lambda$  together with the mapping coefficients. The parametric equation of the shapes then has the form

$$x(\theta) = \frac{\lambda - \operatorname{Re} \omega(\pi) + \operatorname{Re} \omega(\theta)}{F}, \quad y(\theta) = \frac{\operatorname{Im} \omega(\theta)}{F} \quad \text{for } 0 \leq \theta \leq 2\pi, \quad (7.1)$$

$\lambda$	$d_1$	$d_3$	$d_5$	$d_7$	$d_9$	$\Delta W$	$\lambda/h$
0.2	-0.2067	-0.1144	0.0240	0.0067	-0.0033	0.8409	0.2195
0.4	-0.1600	-0.1222	0.0187	0.0081	-0.0033	0.8261	0.4425
0.6	-0.1567	-0.1244	0.0167	0.0086	-0.0022	0.8268	0.6643
0.8	-0.1533	-0.1244	0.0160	0.0090	-0.0022	0.8341	0.8850
1.0	-0.1167	-0.1333	0.0080	0.0090	-0.0015	0.8434	1.1108
1.5	-0.1033	-0.1378	0.0047	0.0071	-0.0015	0.8651	1.6717
2.0	-0.0667	-0.1378	0.0033	0.0071	-0.0007	0.8822	2.2350
3.0	-0.0267	-0.1378	0.0013	0.0071	-0.0004	0.9010	3.3529

**Table 5.** Mapping coefficients, energy increment and the separation ratio  $\lambda/h$  for the optimal shapes at  $M = 9$ . The even terms  $d_{2m}, m = 1, 2, \dots$  go to zero.

where

$$\omega(\theta) = t + \sum_{m=1,3,\dots}^M d_m t^{-m}, \quad F = 1 - \sum_{m=1,3,\dots}^M m d_m^2, \quad t = \exp i\theta.$$

The displacements (2.14) and the stresses (2.15) along the optimal shape can also be obtained through  $\varphi(t)$  and  $\varphi'(t)$ , respectively, as a by-product of the energy optimization. The remaining figures show them as a function of the contour arc length  $s$ :

$$ds = |\omega'(\xi)| |d\xi| = |\omega'(\vartheta)| d\vartheta; \quad \xi = e^{i\vartheta} \in \gamma, \tag{7.2}$$

normalized by the length  $s_0$  of the upper half of the optimal rectangle. Let the contour be traversed in the counterclockwise direction and let  $s = 0$  correspond to the right point on the  $x$ -axis. Let also  $s_1, s_2$  denote the arc length at the upper right and upper left corner points, respectively, so that with a certain approximation we have, setting  $t = x + iy \in L$ ,

$$\begin{aligned} 0 \leq s < s_1 : ds &= dy, & dt &= i dy, \\ s_1 < s < s_2 : ds &= -dx, & dt &= -dx, \\ s_2 < s \leq s_0 : ds &= -dy, & dt &= idy. \end{aligned} \tag{7.3}$$

In stating (7.3) the optimal shape is supposed to be a true rectangle. From Figure 7 we may conservatively conclude that the Cartesian displacements of the optimal shape tend to piecewise linear functions in the corresponding coordinates:

$$\begin{aligned} 0 \leq s < s_1 : u_x(t) &= \alpha_1, \\ s_1 < s < s_2 : u_x(t) &= \alpha_2 x + \alpha_3, \\ s_2 < s \leq s_0 : u_x(t) &= \alpha_4, \\ 0 \leq s < s_1 : u_y(t) &= \beta_1 y + \beta_2, \\ s_1 < s < s_2 : u_y(t) &= \beta_3, \\ s_2 < s \leq s_0 : u_y(t) &= \beta_4 y + \beta_5, \end{aligned} \tag{7.4}$$

where the constants  $\alpha_j, \beta_j$  provide the continuity of displacement at the corners  $s_1, s_2$ . Now, referring back to the displacement-stress relation (2.16) and making use of (7.3) and (7.4), we conclude that the

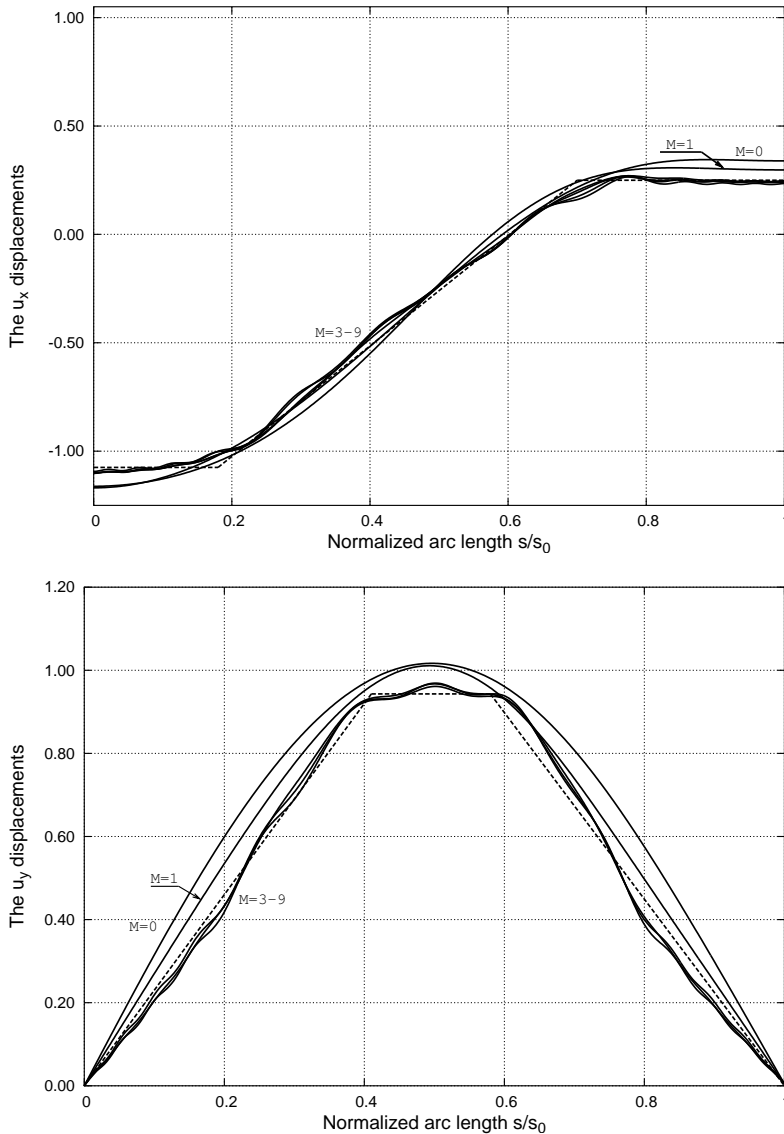


**Figure 7.** Boundary displacements  $u_x(s)$  (top) and  $u_y(s)$  (bottom) along the energy-minimizing hole shape as a function of the mapping size  $M$ , for  $\lambda = 0.4$ . The dashed piecewise linear trend line is also added for comparison.

tangential stresses should be then piecewise constant:

$$\begin{aligned}
 0 \leq s < s_1 : \sigma_{\tau\tau}(s) &= 4q\beta_1, \\
 s_1 < s < s_2 : \sigma_{\tau\tau}(s) &= -4q\alpha_2, \\
 s_2 < s \leq s_0 : \sigma_{\tau\tau}(s) &= 4q\beta_4,
 \end{aligned} \tag{7.5}$$

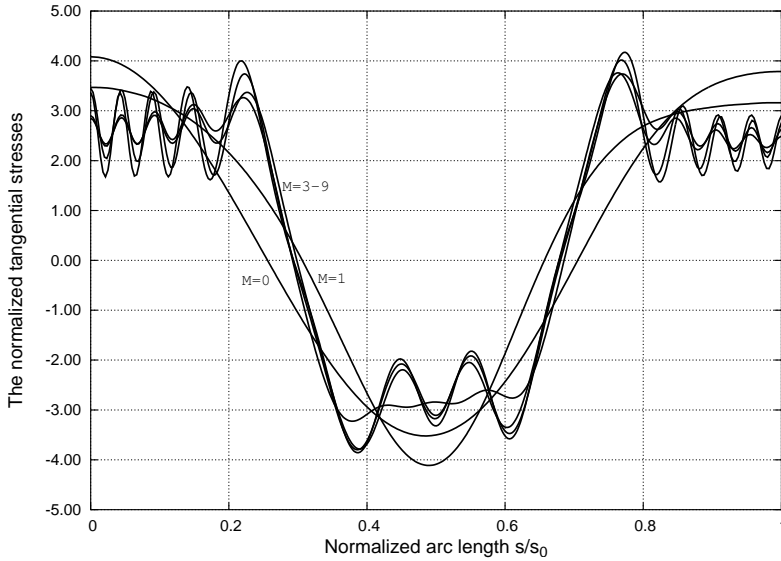


**Figure 8.** Tangential stresses  $\sigma_{\tau\tau}(s)$  along the energy-minimizing hole shape as a function of the mapping size  $M$  at  $\lambda = 0.4$ .

where we introduced the symbol

$$q = \left( \frac{1}{K} + \frac{1}{\mu} \right)^{-1}.$$

However, the stress distributions obtained through (2.15) independently of the linearity assumption (7.4) on the displacements exhibit, for  $M \geq 2$ , unacceptable oscillations (Figure 8) that mask the piecewise constancy trend. They result from numerical term-by-term differentiation, as explained at the end of Section 4.

To improve the situation, we smooth the stresses so computed by numerical expansion in Fourier series followed by convolution with the Feier kernel. Though crude, this analysis shows that the filtered stresses (Figure 9) tend to a piecewise distribution. These numerical conjectures are in keeping with the already known analytical facts that the Cartesian displacements of equistress boundaries are proportional to the corresponding coordinate [Vigdergauz 1988] and that the stress distribution along the optimal shape of a single hole under pure shear is piecewise constant [Vigdergauz and Cherkayev 1986]. Further, Figures 8 and 9 show that the energy minimization with increasing  $M$  is accompanied by decreasing the stress concentration. This favors our choice of the energy optimization.

In this context, very interesting results have been independently obtained by Waldman et al. [2003] through FEM analysis within an effective gradientless optimization searching. The quadrangle-like interacting holes were numerically shown to keep the stress constancy which was taken as the optimization criterion. Figure 10 shows a quantitative agreement between the stress distribution along the stress-minimizing [Waldman et al. 2003] and the energy-minimizing holes at shear type (but not pure shear) loading  $\Gamma_0/2B_0 = 3$  and at approximately the same hole separation. The observed stress concentration error of 8-9% stems not only from the lesser accuracy of the KM energy solver in computing the stresses

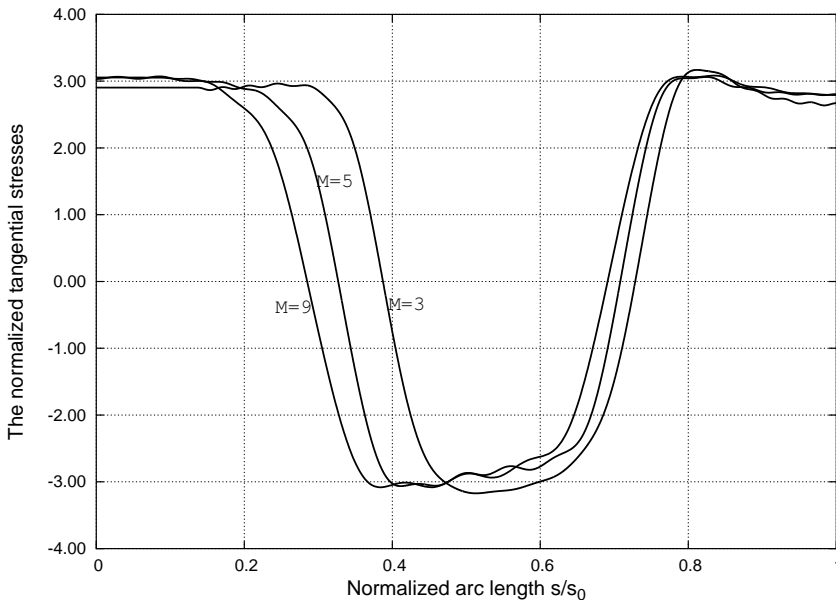


**Figure 9.** Filtered stress distributions  $\sigma_{\tau\tau}(s)$  along the energy-minimizing hole shape as a function of the mapping size  $M$  at  $\lambda = 0.4$ .

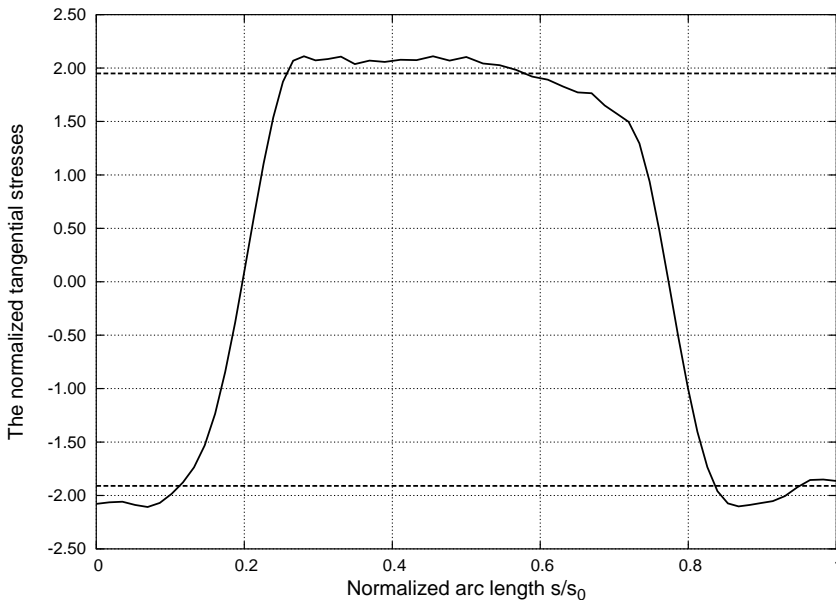


**Figure 10.** Filtered stress distributions  $\sigma_{\tau\tau}(s)$  along the energy-minimizing hole at  $\lambda/h \approx 0.322$  and  $\Gamma_0/2B_0 = 3$  against the stress constancy optimization levels (the dashed lines) along the quadrangle sides [Waldman et al. 2003].

but also, to some extent, from comparing the *energy*-minimizing hole in an *infinite* plane to the *stress*-constant hole in a *finite* plate. For reference, we also note that the constant-stress value  $|\sigma| = 2.84$  reported in [Waldman et al. 2003] for a single hole under pure shear deviates by approximately 2% from the semianalytical value 2.779... [Vigdergauz 2006].

## 8. Concluding remarks

The essential points in this paper are, first, the novel utilization of the conformal mapping technique to encode the optimized shapes within an evolutionary algorithm and, second, the effective application of this scheme to the rather difficult optimization problem of two-dimensional elastostatics.

In our opinion, the proposed mapping-based shape representation can be a competitive alternative to the nodal points in numerically treating both forward and optimization boundary-value problems of continuum mechanics. This computation-saving technique is easily adapted to evaluate appearing boundary integrals in a variety of direct solvers, from ideally suited integral equations to less open FEMs.

The specific results obtained show that interacting holes under pure shear store less energy and hence are stiffer than a single hole of the same area. Though known as rule-of-thumb, this fact has not yet been investigated numerically. It is of special interest that the stress concentration on the stress-constant holes is numerically shown to be independent of the separation distances [Waldman et al. 2003].

## References

- [Alfors 1979] L. Alfors, *Complex analysis*, 3rd ed., McGraw-Hill, New York, 1979.
- [Banichuk 1977] N. V. Banichuk, “Optimality conditions in the problem of seeking the hole shapes in elastic bodies”, *J. Appl. Math. Mech.* **41** (1977), 920–925. [MR 80i:73012](#)
- [Cherepanov 1974] G. P. Cherepanov, “Inverse problems of the plane theory of elasticity”, *Prikl. Mat. Mekh.* **38**:6 (1974), 963–979. In Russian; translated in *J. Appl. Math. Mech.* **38**:5 (1974), 913–931. [MR 52 #7254](#)
- [Cherkaev et al. 1998] A. V. Cherkaev, Y. Grabovsky, A. B. Movchan, and S. K. Serkov, “The cavity of the optimal shape under the shear stresses”, *Internat. J. Solids Structures* **35**:33 (1998), 4391–4410. [MR 99e:73040](#)
- [Cherkaev n.d.] A. V. Cherkaev, “Optimal shapes of holes in an elastic plane”, Web page, n.d., See <http://www.math.utah.edu/~cherk/holes/index.html>.
- [England 1971] A. H. England, *Complex variable methods in elasticity*, Wiley, London, 1971. Reprinted by Dover, New York, 2003. [MR 57 #4745](#)
- [Gibiansky and Cherkaev 1984] L. V. Gibiansky and A. V. Cherkaev, “Design of composite plates of extremal rigidity”, Report 914, Ioffe Physicotechnical Institute, Leningrad, 1984. In Russian; translated as pp. 95–137 in *Topics in the mathematical modelling of composite materials*, edited by A. V. Cherkaev and R. H. Kohn, Progr. Nonlinear Differential Equations Appl. **31**, Birkhäuser, Boston, 1997. [MR 1493041](#)
- [Grabovsky and Kohn 1995] Y. Grabovsky and R. V. Kohn, “Microstructures minimizing the energy of a two phase elastic composite in two space dimensions, II: The Vigdergauz microstructure”, *J. Mech. Phys. Solids* **43**:6 (1995), 949–972. [MR 96c:73043](#)
- [Helsing and Jonsson 2000] J. Helsing and A. Jonsson, “Complex variable boundary integral equations for perforated infinite planes”, *Engineering Analysis with Boundary Elements* **25**:3 (2000), 191–202.
- [Jasiuk 1995] I. Jasiuk, “Cavities vis-a-vis rigid inclusions: elastic moduli of materials with polygonal inclusions”, *International Journal of Solids and Structures* **32**:3/4 (1995), 407–422.
- [Ling 1948] C.-B. Ling, “On the stresses in a plate containing two circular holes”, *J. Appl. Phys.* **19** (1948), 77–82. [MR 9,395k](#)

- [Muskhelishvili 1963] N. I. Muskhelishvili, *Some basic problems of the mathematical theory of elasticity: Fundamental equations, plane theory of elasticity, torsion and bending*, Noordhoff, Leyden, 1963. [MR 50 #15516](#)
- [Osyczka 2001] A. Osyczka, *Evolutionary algorithms for single and multicriteria design optimization*, Springer, Heidelberg, 2001.
- [Schoenauer et al. 1996] M. Schoenauer, L. Kallel, and F. Jouve, “Mechanical inclusions identification by evolutionary computation”, *Rev. Européenne Élé. Finis* **5**:5-6 (1996), 619–648. [MR 97m:73060](#)
- [Ting et al. 1999] K. Ting, K. T. Chen, and W. S. Wang, “Applied alternating method to analyze the stress concentration around interacting multiple circular holes in an infinite domain”, *International Journal of Solids and Structures* **36** (1999), 533–556.
- [Vigdergauz 1976] S. B. Vigdergauz, “Integral equation of the inverse problem of the plane theory of elasticity”, *Prikl. Matem. Mekhan.* **40** (1976), 566–569. In Russian; translated in *Journal of Applied Mathematics and Mechanics* **40**:3 (1976), 518–522.
- [Vigdergauz 1982] S. B. Vigdergauz, “Equi-strength hole in a half-plane”, *Izv. AN SSSR, Mekhanika Tverdogo Tela* **17** (1982), 94–98. In Russian; translated in *Mechanics of Solids* **17**:1 (1982), 87–91.
- [Vigdergauz 1988] S. B. Vigdergauz, “Stressed state of an elastic plane with constant-stress holes”, *Izv. AN SSSR, Mekhanika Tverdogo Tela* **23** (1988), 101–104. In Russian; translated in *Mechanics of Solids* **23**:3 (1988), 96–99.
- [Vigdergauz 1996] S. B. Vigdergauz, “Rhombic lattice of equi-stress inclusions in an elastic plate”, *Quart. J. Mech. Appl. Math.* **49**:4 (1996), 565–580. [MR 97g:73074](#)
- [Vigdergauz 2001a] S. B. Vigdergauz, “Genetic algorithm perspective to identify energy-optimizing inclusions in an elastic plate”, *International Journal of Solids and Structures* **38** (2001), 6851–6867.
- [Vigdergauz 2001b] S. B. Vigdergauz, “The effective properties of a perforated elastic plate: Numerical optimization by genetic algorithm”, *International Journal of Solids and Structures* **38** (2001), 8593–8616.
- [Vigdergauz 2006] S. B. Vigdergauz, “Stress-minimizing hole in an elastic plate under remote shear”, *Journal of Mechanics of Materials and Structures* **1** (2006), 387–406.
- [Vigdergauz and Cherkayev 1986] S. B. Vigdergauz and A. V. Cherkayev, “A hole in a plate optimal for its biaxial extension-compression”, *Prikl. Mat. Mekh.* **50**:3 (1986), 524–528. In Russian; translated in *J. Appl. Math. Mech.* **50**:3 (1986), 401–404. [MR 88g:73073](#)
- [Waldman et al. 2003] W. Waldman, M. Heller, and L. R. F. Rose, “[Shape optimisation of two closely spaced holes for fatigue life extension](#)”, Report dsto-rr-0253, Defence Science and Technology Organization, Department of Defence, Australian Government, 2003, See <http://www.dsto.defence.gov.au/publications/2558/>.

Received 2 Mar 2008. Revised 23 Jun 2008. Accepted 26 Jun 2008.

SHMUEL VIGDERGAUZ: [smuel@iec.co.il](mailto:smuel@iec.co.il)

Research and Development Division, The Israel Electric Corporation, Ltd., P. O. Box 10, Haifa 31000, Israel